DEVELOPMENT AND CHARACTERIZATION OF XYLAN-CHITOSAN COATED ZEIN NANOPARTICLES FOR COLON-TARGETED DIOSMETIN DELIVERY

AVIKUMAR BAWANKAR and LAXMIKANT ZAWAR

Department of Pharmaceutics, H. R. Patel Institute of Pharmaceutical Education and Research, Shirpur 425405, Maharashtra State, India
✉ *Corresponding author:L. R. Zawar, shwet.zawar@gmail.com*

Received March 17, 2026

The use of diosmetin (Dio), a bioactive flavonoid with antioxidant and anticancer potential for colon disorders, is limited by its poor solubility and bioavailability. This study developed a colon-targeted delivery platform by encapsulating Dio in zein (Zn) nanoparticles with xylan (Xy) and chitosan (Chi) coatings for pH- and enzyme-responsive release. Dio-loaded Zn nanoparticles were produced by antisolvent nanoprecipitation, followed by Xy and Chi coating (0.01–1.0% w/v). Formulations were characterized using DLS/zeta potential, SEM, FTIR, DSC, and PXRD, with drug loading quantified by UV–vis. The optimized Zn:Dio:Xy:Chi ratio (1:1:1) produced spherical nanoparticles of 548 nm (PDI ~0.26) with zeta potential changing from −21.25 mV to +41.10 mV after coating, indicating successful modification. Xy/Chi coating increased encapsulation efficiency to 92.82%, while reducing loading capacity to 9.28% due to added mass. FTIR, DSC, and PXRD confirmed drug-polymer interactions without degradation; SEM showed coated architecture. Coated nanoparticles demonstrated thermal, ionic, pH, and storage stability. In simulated digestion, Zn–Dio–Xy/Chi limited release in SGF (9.30%) and SIF (29.25%), but enabled higher release in SCF (63.19%/24 h), following Higuchi kinetics (R^2=0.9782). This nanocarrier system offers a promising platform for colon-specific drug delivery.

Keywords: natural polymer, zein, diosmetin, xylan, chitosan, drug release

INTRODUCTION

Natural phytochemicals, which are secondary metabolites derived from plants, possess diverse biological activities, including antioxidant, anti-inflammatory, antimicrobial, and anticancer properties. These attributes make them promising candidates for therapeutic and nutraceutical applications. Diosmetin (Dio) (5,7,3′-trihydroxy-4′-methoxyflavone) is a naturally occurring monomethoxyflavone widely present in citrus peels and several medicinal plants. It has demonstrated significant antioxidant, anti-inflammatory, and anticancer activities in various preclinical studies.[1,2] However, the clinical application of Dio is limited by its poor aqueous solubility, low gastrointestinal absorption, and consequently reduced oral bioavailability,[3] which may restrict its effective utilization following oral administration. Therefore, an appropriate delivery system capable of improving the physicochemical and biopharmaceutical properties of Dio needs to be developed.

Nanoparticle-based delivery systems provide an effective strategy to overcome such limitations by enhancing drug solubility, protecting bioactive compounds from degradation, enabling controlled release, and facilitating targeted delivery.[4,5] Among the various nanocarrier materials, biopolymer-based nanoparticles have received particular attention due to their biodegradability, biocompatibility, and ability to incorporate hydrophobic compounds.

Zein (Zn), a hydrophobic prolamin protein obtained from corn, is widely recognized as a biodegradable and biocompatible carrier for encapsulating lipophilic bioactive compounds. Zn-based nanoparticles prepared using techniques such as nanoprecipitation have shown improved stability, drug loading efficiency, and controlled release behavior for hydrophobic drugs.[6]

However, unmodified zein nanoparticles may have limited functionality under the complex gastrointestinal environment, particularly with respect to surface properties, colloidal stability, and site-specific drug release. Consequently, surface modification of zein nanoparticles represents a promising strategy for further optimizing their performance as oral delivery systems.

Surface modification of Zn nanoparticles with polysaccharides or polycations can further enhance their functional properties. Chitosan (Chi), a positively charged polysaccharide, provides excellent mucoadhesive characteristics and can transiently open epithelial tight junctions, thereby enhancing interaction with the colonic mucosa and prolonging gastrointestinal residence time.[7-9] In addition, xylan (Xy), an anionic polysaccharide degradable by colonic microbiota, can be used to achieve enzyme-triggered colon-specific drug release. A multilayer coating strategy combining Xy and Chi on a Zn nanoparticle core may therefore provide protection in the upper gastrointestinal tract, while enabling targeted drug release in the colon through microbiota-mediated degradation and enhanced mucosal interaction.[10] Thus, the combination of Xy and Chi as a surface coating on a Zn-based nanoparticle may provide complementary functional characteristics, with the polysaccharide layer potentially contributing to gastrointestinal protection, modulation of surface properties, and microbiota-associated release of the encapsulated drug in the colon. Such a core–shell architecture may therefore offer advantages over an uncoated zein nanoparticle for site-specific delivery.

Previous studies have investigated protein-based nanoparticles for the encapsulation of bioactive compounds and the use of Chi-based surface coatings to modify nanoparticle stability and delivery characteristics.[11] However, the integration of a Dio-loaded Zn core with sequential Xy and Chi coating for colon-targeted delivery remains unexplored. The present study addresses this research gap through the rational combination of three functionally distinct biopolymers within a single nanoparticulate system: Zn as the hydrophobic matrix for Dio encapsulation, Xy as a microbiota-degradable polysaccharide, and Chi as a surface-modifying and mucoadhesive polymer. The novelty therefore lies not merely in the individual use of these materials, but in their sequential organization as a Zn-Dio-Xy/Chi system intended to couple drug encapsulation and upper gastrointestinal protection with controlled release under simulated colonic conditions. In addition, the contribution of the Xy/Chi coating was systematically examined through comparison of the physicochemical characteristics, thermal behaviour, and colloidal stability under varying pH and ionic-strength conditions, together with drug-release behaviour under sequential simulated gastrointestinal and colonic environments.

Accordingly, the present study aimed to develop and characterize Dio-loaded Zn nanoparticles sequentially coated with Xy and Chi (Zn-Dio-Xy/Chi) as a biopolymer-based nanocarrier for colon-targeted delivery.[12–14] The developed system was evaluated for particle size, polydispersity, surface charge, drug encapsulation and loading, morphological and solid-state characteristics, and stability under thermal, ionic, pH, and storage conditions. Its release behaviour was further investigated under sequential simulated gastric, intestinal, and enzyme-containing colonic conditions to determine whether the Xy/Chi coating could restrict premature Dio release in the upper gastrointestinal environment, while facilitating controlled release under simulated colonic conditions.

EXPERIMENTAL

Materials

Diosmetin (Dio % 98.0%), Zein (Zn, MW: 25-40 kDa), Xylan (Xy) and Chitosan (Chi) was obtained from TCI Chemical, Pvt. Ltd., India, and bile salt were supplied by Sisco Research Lab. Pvt. Ltd., Mumbai, India. Pepsin (1:3000) was procured from Loba Chemie Pvt. Ltd. Mumbai, India. Hydrochloric acid (36%), sodium hydroxide were supplied by Merck; xylanase, chitosinase and betaglucosidase were procured from Shughengheng Jiangsu Chemical Company, China.

Preparation of Zn-Dio-Xy/Chi nanoparticles

Initially, Zn-Dio nanoparticles were successfully formulated employing the antisolvent precipitation method.[15] 'Zn' (150 mg) and 'Dio' (50 mg) were dissolved in 30 mL of 83% ethanol-water (v/v) and stirred magnetically at 600 rpm for 30 min. The solution was added dropwise to 250 mL of deionized water at pH 3.0 (0.1N HCL) under continuous stirring for 1 h to form Zn-Dio nanoparticles, followed by ethanol removal using a rotary evaporator at 40 °C. For coating, Zn-Dio nanoparticles were added dropwise into 125 mL of Xy solution (0.01-1.0% w/v) under stirring (300 rpm) on a magnetic stirrer to form Zn-Dio-Xy nanoparticles, which were subsequently added dropwise into 125 mL of Chi solution (0.01-1.0% w/v, pH 4) maintaining identical stirring parameters to obtain Zn-Dio-Xy/Chi nanoparticles.

Characterization of nanoparticles

Spectral analysis

Particle size, polydispersity index (PDI), and zeta potential were measured at 25 °C using a Nanoplus3 particle size and zeta analyzer (Micromeritics, USA) at a 90° scattering angle.[4]

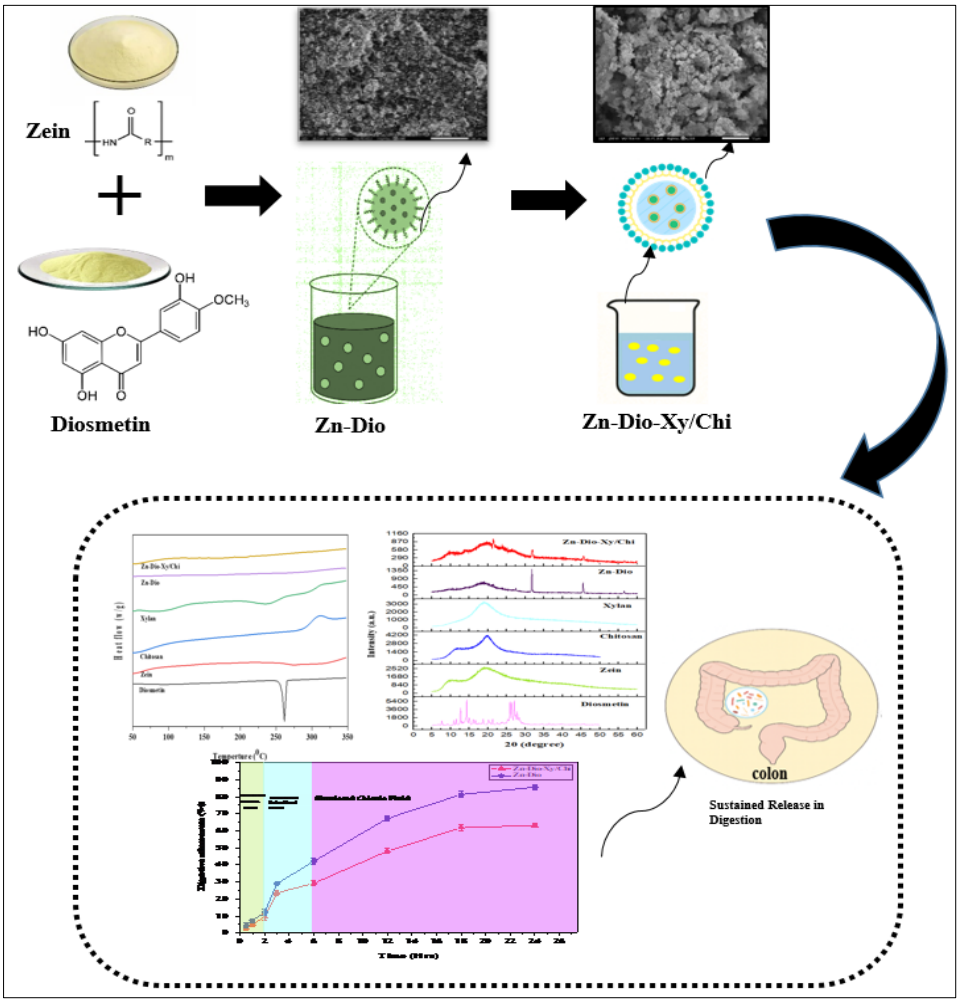


Figure 1: Xylan-chitosan coated zein nanocarriers for colon-targeted diosmetin delivery

The surface morphology of the nanoparticles was examined using scanning electron microscopy (SEM; JEOL JSM-6390 LV, USA, TEM; Talos L120C G2, ThermoFisher). Fourier transform infrared (FTIR) spectroscopy (Bruker Vertex 70, Alpha-II) was employed to analyze chemical composition and molecular interactions. The thermal behavior of Dio, Zn, Xy, Chi, Zn–Dio, and Zn–Dio–Xy/Chi nanoparticles was evaluated using differential scanning calorimetry (DSC; TA Instruments, USA). Samples were sealed in aluminum pans and heated from 50 to 280 °C at a heating rate of 10 °C min^{-1}.[4]

Powder X-ray diffraction (PXRD) analysis was carried out using a Bruker D8 wide-angle diffractometer (Bruker, Germany) equipped with Cu–Kα radiation (λ = 0.15418 nm) generated from a copper anode operating at 40 kV and 40 mA. Diffractograms were recorded by continuous scanning at 5° min^{-1} over a 2θ range of 0°–50°.

FTIR spectra of Dio, Zn, Xy, Chi, Zn–Dio, and Zn–Dio–Xy/Chi nanoparticles were recorded at 25 °C over a wavenumber range of 400–4000 cm^{-1}.

Loading capacity (LC) and encapsulation efficiency (EE)

The encapsulation efficiency and loading capacity of Dio in Zn-Dio-Xy/Chi nanoparticles were evaluated.[11] Freshly prepared Zn-Dio-Xy/Chi samples were centrifuged at 8000 rpm for 30 min, after which they were diluted an 80% ethanol aqueous solution to achieve the desired concentration. The absorbance of the resulting solution was measured at 348 nm using UV-vis spectroscopy. Finally, the 'Dio' concentration in Zn-Dio-Xy/Chi nanoparticles was determined as an LC (%) and EE (%) using Equations (1) and (2):

$$\text{EE (\%)} = \frac{\text{Total Dio mass (mg)} - \text{free Dio mass (mg)}}{\text{Total Dio mass (mg)}} \times 100 \quad (1)$$

$$\text{LC (\%)} = \frac{\text{Total Dio mass (mg)} - \text{free Dio mass (mg)}}{\text{Total mass of nanoparticles}} \times 100 \quad (2)$$

Stability evaluation

Stability studies of the Zn-Dio and Zn-Dio-Xy/Chi nanoparticles were conducted to evaluate the effects of pH, temperature variation, ionic strength, and storage duration. Freshly prepared nanoparticle dispersions (10 mL each, n=3) were incubated at different temperatures (40, 50, 60, 70, 80, and 90 °C) for 45 min in a controlled water bath. After thermal treatment, all samples were allowed to return to ambient temperature prior to further evaluation. The stability of the nanoparticles was assessed by measuring the particle size and zeta potential. Freshly prepared Zn-Dio and Zn-Dio-Xy/Chi nanoparticle dispersions (10 mL each) were subjected to continuous stirring for 20 min in the presence of varying NaCl concentrations (10, 20, 50, 100, and 200 mmol/L) to assess ionic strength stability. The resulting samples were analyzed for particle size and zeta potential.[13,14] To evaluate pH stability, freshly prepared nanoparticle suspensions (10 mL each) were adjusted to pH values ranging from 4 to 8 using 0.1 M NaOH and 0.1 M HCl solutions. The suspensions were equilibrated for 10 min before measurement, followed by particle size and zeta potential analysis. Finally, to investigate long-term storage stability, the Zn-Dio and Zn-Dio-Xy/Chi nanoparticles were stored at 2–8 °C. Samples were collected weekly and evaluated at room temperature (25 °C) to monitor changes in particle size and zeta potential over time.

***In vitro* simulated gastrointestinal digestion**

The *in vitro* gastrointestinal digestion of the synthesized nanoparticles was simulated using the dialysis membrane method to mimic physiological digestive conditions.[15] Briefly, dispersions of Zn-Dio and Zn-Dio-Xy/Chi nanoparticles in deionized water were separately placed into dialysis bags, which were tightly sealed to prevent nanoparticle leakage. The bag was immersed in 150 mL of simulated gastric fluid (SGF) prepared by dissolving 2 mg/mL NaCl and 3.2 mg/mL pepsin, with the pH adjusted to 1.2 using 1 M HCl. The system was maintained at 37 °C under constant agitation for 1 h to simulate gastric digestion. Following this, the dialysis bags were transferred into 150 mL of simulated intestinal fluid (SIF; pH 6.8), formulated by dissolving 8.8 mg/mL NaCl, 6.8 mg/mL KH_2PO_4, and 2.0 mg/mL bile salts, with pH adjustment using 1 M HCl. After intestinal digestion, the bags were further moved into 150 mL of simulated colonic fluid (SCF; pH 7.4), prepared by dissolving 8.8 mg/mL NaCl, 6.8 mg/mL KH_2PO_4, 0.0166 mg/mL xylanase, 1.75 mg/mL chitosanase, and 0.25 mg/mL β-glucosidase, with pH adjustment using 1 N NaOH. During the digestion study, 5 mL aliquots were withdrawn at predetermined time intervals of 0.5, 1, 2, 3, 6, 12, 18, and 24 h, while maintaining the samples in a water bath shaker at 37 °C and 100 rpm. To preserve sink conditions, an equal volume of fresh buffer was added after each withdrawal. The concentration of Dio released at each sampling point was quantified as described in Equation (3):

$$\text{Digestive release rate (\%)} = \frac{\text{Wt of released Dio (mg)}}{\text{Wt of Dio before digestion (mg)}} \times 100 \quad (3)$$

Statistical analysis

Each experiment was performed in triplicate, and the results were presented as the mean ± standard deviation (SD). Statistical significance was set at $p < 0.05$. Statistical analyses, including one-way analysis of variance (ANOVA), were used to identify significant differences between the experimental groups.

RESULTS AND DISCUSSION

Particle size, polydispersity index (PDI), and zeta potential analysis

Figure 2A illustrates the particle size distribution and corresponding polydispersity index (PDI) values of the Zn, Zn-Dio, and Zn-Dio-Xy/Chi nanoparticle formulations. The Zn nanoparticles exhibited an average particle diameter of 180.1 nm with a PDI of 0.18, indicating a relatively narrow size distribution and good colloidal uniformity. In contrast, the Zn-Dio nanoparticles showed an increased mean particle size of 350.4 nm with a PDI of 0.23. The increase in particle size following drug incorporation may be attributed to strong hydrophobic interactions between the nonpolar regions of Dio and the hydrophobic amino acid residues present in the Zn matrix. These interactions can promote molecular association and partial crosslinking within the nanoparticle core, leading to the formation of a denser and more stabilized nanostructure during the antisolvent precipitation process.[16]

Further modification of the nanoparticles with Xy/Chi coatings resulted in a substantial increase in particle size. Compared with the Zn and Zn-Dio systems, the Zn-Dio-Xy/Chi nanoparticles exhibited mean particle diameters ranging from 548 nm (PDI 0.26) to 920 nm (PDI 0.29) as the concentration of the Xy/Chi coating increased from 50 mg to 100 mg. This enlargement in particle size can be primarily attributed to electrostatic interactions between the surface charges of the Zn-based nanoparticles and the functional groups present in the Xy/Chi biopolymer coating. These interactions facilitate the formation of a polysaccharide-based shell surrounding the nanoparticle core, thereby increasing the overall hydrodynamic diameter of the system.[17,18]

Additionally, the presence of polysaccharide chains may induce partial nanoparticle aggregation

through a polymer-bridging mechanism, where individual polymer chains interact simultaneously with multiple nanoparticles. Such bridging interactions can connect adjacent particles, resulting in the formation of larger composite structures and contributing to the observed increase in particle size.[19,20] Despite the increase in size, the PDI values remained below 0.30, indicating that the formulations maintained a reasonably uniform size distribution suitable for nanoparticle-based drug delivery systems. Zeta potential measurements revealed a significant alteration in surface charge following the Xy/Chi coating process, as shown in Figure 2B. The Zn nanoparticles exhibited a positive zeta potential of +18.20 mV, whereas the uncoated Zn-Dio nanoparticles displayed a negative zeta potential of −21.25 mV. This shift toward a negative charge is likely associated with the ionization of functional groups present in the formulation, including carboxyl groups from Zn and phenolic hydroxyl groups of Dio, which contribute to the overall surface charge of the nanoparticles.

Upon coating with Xy/Chi, the zeta potential shifted markedly to a positive value of +41.10 mV. This change is primarily attributed to the presence of protonated amino groups of Chi, which impart a strong positive surface charge, along with the polysaccharide framework provided by Xy. The reversal and significant increase in surface charge confirm the successful deposition of the Xy/Chi coating layer on the nanoparticle surface.

The high positive zeta potential also suggests improved colloidal stability, as strong electrostatic repulsion between particles can prevent aggregation and maintain nanoparticle dispersion. Moreover, the positively charged surface may enhance mucoadhesive interactions with negatively charged mucosal surfaces and facilitate improved cellular uptake, which are desirable characteristics for colon-targeted drug delivery systems. Collectively, these results demonstrate that the Xy-Chi coating acts as an effective biocompatible stabilizing layer, improving both the physicochemical stability and functional performance of Zn-based nanoparticles for targeted drug delivery applications.

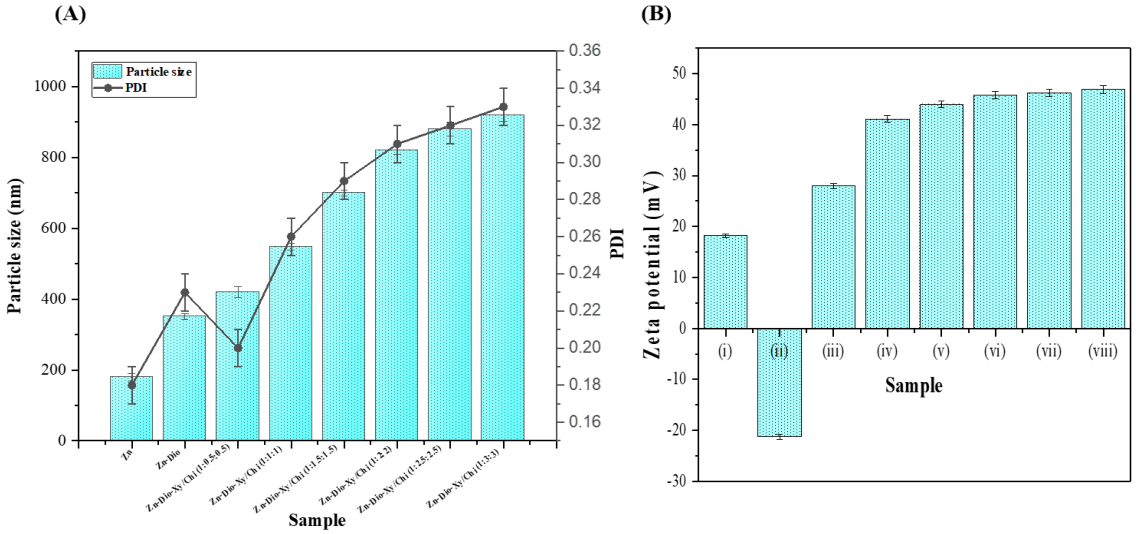


Figure 2: (A) Particle size and polydispersity index (PDI) measurements. (B) Zeta-potential analysis of (i) Zn, (ii) Zn-Dio, (iii) Zn-Dio-Xy/Chi (1:0.5:0.5), (iv) Zn-Dio-Xy/Chi (1:1:1), (v) Zn-Dio-Xy/Chi (1:1.5:1.5), (vi) Zn-Dio-Xy/Chi (1:2:2), (vii) Zn-Dio-Xy/Chi (1:2.5:2.5) and (viii) Zn-Dio-Xy/Chi (1:3:3) nanoparticles

Loading capacity and encapsulation efficiency

Figure 3A presents the encapsulation efficiency (%EE) and loading capacity (%LC) of Dio in Zn-Dio and Zn-Dio-Xy/Chi nanoparticle formulations. The Zn-Dio nanoparticles exhibited an encapsulation efficiency of 85.0 ± 0.14%, indicating effective incorporation of Dio within the Zn matrix. Following surface coating with the Xy/Chi polysaccharide system, the encapsulation efficiency increased significantly to 92.82 ± 0.09%. This enhancement suggests that the presence of the polysaccharide coating improved the retention of Dio within the nanoparticle structure, likely by forming an additional protective layer around the drug-loaded core.

Notably, when the Zn:Xy/Chi mass ratio reached 1:1:1, the encapsulation efficiency achieved its highest value (92.82 ± 0.09%). This

observation indicates that the formation of a relatively thicker Xy/Chi coating layer may act as an effective diffusion barrier, thereby minimizing drug leakage from the nanoparticle core during preparation and subsequent handling. The simultaneous increase in particle size observed for the coated formulations further supports the successful deposition of the Xy/Chi layer on the nanoparticle surface.

The loading capacity (%LC) values for the Zn-Dio and Zn-Dio-Xy/Chi nanoparticles were determined to be 22.08 ± 0.02% and 9.28 ± 0.02%, respectively. The reduction in %LC with increasing Xy/Chi content can be attributed to the increased total mass of the nanoparticle system after coating. Although the amount of encapsulated Dio within the core remained relatively constant, the addition of the polysaccharide shell significantly contributed to the overall particle weight, thereby reducing the calculated proportion of drug relative to the total nanoparticle mass.

These findings suggest the presence of strong electrostatic and intermolecular interactions between the Xy/Chi polymers and the Zn nanoparticle surface, facilitating the formation of a stable core–shell nanostructure capable of effectively entrapping Dio. Such structural organization not only improves drug retention, but may also contribute to enhanced stability and controlled drug release behavior. Based on the combined evaluation of particle size, PDI, zeta potential, %EE, and %LC, the optimized nanoparticle formulation was identified at a Zn:Xy/Chi mass ratio of 1:1:1, which provided the most favorable balance between encapsulation efficiency, stability, and structural characteristics.[21,22]

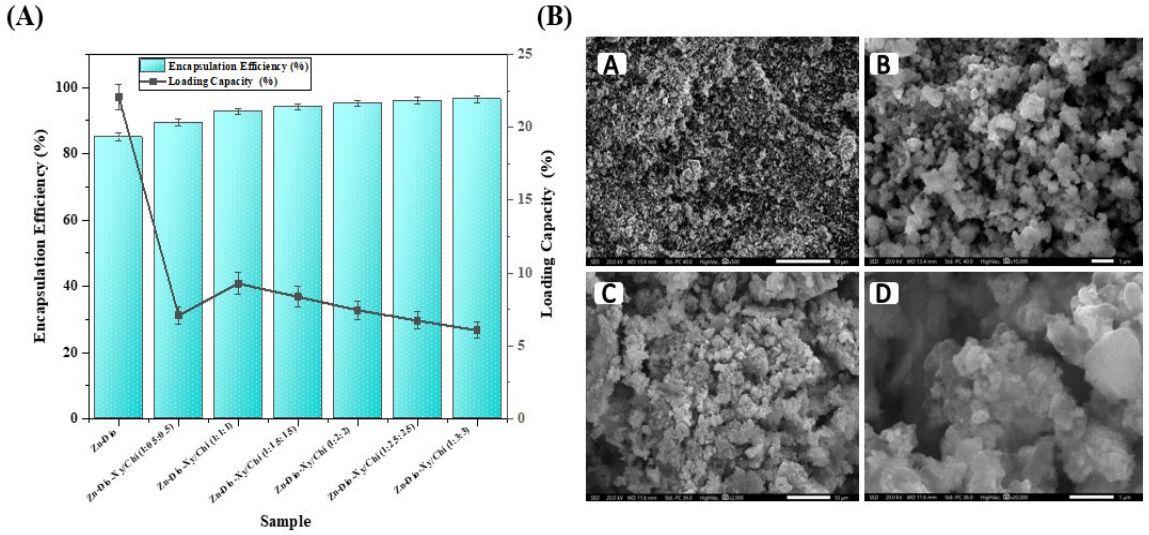


Figure 3: Loading capacity and encapsulation efficiency (A) and SEM of Zn-Dio (A, B) and Zn-Dio-Xy/Chi (C, D) nanoparticles

SEM analysis

The surface morphology and microstructural features of the Zn-Dio nanoparticles were examined using scanning electron microscopy (SEM), and the corresponding micrographs are presented in Figure 3B. At lower magnification (×500), the nanoparticles appeared as agglomerated clusters with irregular surface textures. This morphology indicates the inherent tendency of Zn-based nanoparticles to form compact assemblies during the nanoprecipitation process, which can occur due to intermolecular interactions and partial particle aggregation during solvent removal. Importantly, no large crystalline aggregates of Dio were detected in the micrographs, suggesting that the drug was effectively encapsulated and uniformly dispersed within the protein matrix rather than existing as separate crystalline domains.

At higher magnification (×10,000), the Zn-Dio nanoparticles exhibited predominantly spherical to near-spherical shapes with a relatively uniform size distribution. The particle surfaces appeared moderately rough rather than smooth, which is consistent with the incorporation of Dio molecules within or partially exposed at the Zn matrix interface. Such surface roughness may arise from molecular interactions between the hydrophobic regions of Zn and the encapsulated drug during nanoparticle formation. This structural feature can

be advantageous for drug delivery applications, as rough surfaces may increase the effective surface area and facilitate improved drug loading as well as sustained drug release behavior. Overall, the SEM analysis confirms the successful formation of nanoscale Zn-Dio nanoparticles with a morphology suitable for oral and colon-targeted drug delivery applications, supporting the potential of Zn as an effective nanocarrier system for Dio.[4,11]

To further investigate the surface morphology and microstructural characteristics of the polymer-coated system, SEM imaging of the Zn-Dio-Xy/Chi nanoparticles was performed at magnifications of 2,000× and 20,000×. At lower magnification (2,000×), the nanoparticles displayed a densely packed granular architecture with irregularly shaped agglomerates. The particle surfaces appeared rough and porous, suggesting the presence of a high surface area structure. Such morphological characteristics may enhance interactions with the surrounding biological environment and potentially improve drug loading capacity and interfacial interactions. The observed agglomeration is likely associated with the presence of biopolymeric coatings, particularly Chi and Xy, which are known to promote interparticle adhesion through hydrogen bonding and electrostatic interactions between polymer chains.[23]

At higher magnification (20,000×), the SEM micrographs revealed more detailed structural features. Individual nanoparticles became more distinguishable, with clearer particle boundaries and a heterogeneous size distribution. The surface texture exhibited a hierarchical organization composed of smaller structural subunits, which likely resulted from the self-assembly behavior of Zn during nanoparticle formation combined with the encapsulation of Dio within the polymeric network. The observed changes in surface texture and particle morphology are consistent with the incorporation of Chi and Xy as surface-associated polymeric coatings; however, SEM alone cannot definitively resolve or confirm the formation of a distinct core-shell architecture. Such a layered architecture may enhance the structural stability of the nanoparticles, while also contributing to controlled and sustained drug release behavior.

Overall, the SEM analysis demonstrates distinct morphological and surface-textural characteristics of the Zn-Dio-Xy/Chi nanoparticles compared with the uncoated Zn-Dio nanoparticles, supporting the formation of the polymer-associated composite system. These features are particularly important for targeted drug delivery systems, as surface roughness, porosity, and polymeric coatings can significantly influence nanoparticle-biological interactions, including cellular uptake, mucoadhesion, and drug release kinetics.

TEM analysis

The TEM analysis of Zn-Dio nanoparticles revealed the formation of compact nanoscale particulate structures with predominantly irregular to near-ovoid morphology Figure 4A. The particles exhibited relatively high electron density in the central region, indicating the formation of a condensed Zn-Dio/zein nanoparticulate matrix. Some degree of particle aggregation was observed, which may be attributed to interparticle interactions and sample drying during TEM grid preparation. The TEM-observed morphology supports the formation of Zn-Dio nanoparticles and complements the particle-size and polydispersity measurements obtained by dynamic light scattering (DLS).

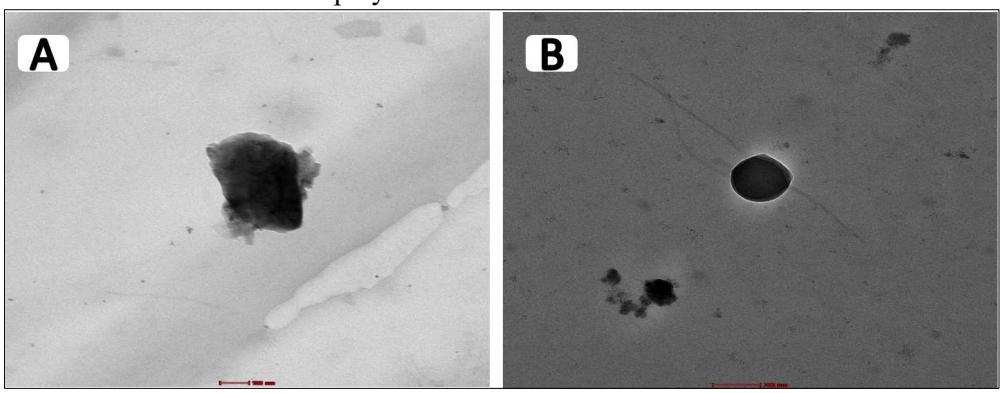


Figure 4: TEM of Zn-Dio (A) and Zn-Dio-Xy/Chi (B) nanoparticles

TEM analysis of Zn-Dio-Xy/Chi nanoparticles demonstrated a distinct compact electron-dense central region surrounded by a comparatively less electron-dense peripheral region Figure 4B. The difference in electron contrast between the central region and the surrounding layer is consistent with a core–shell-like architecture, suggesting the deposition of the Xy/Chi coating around the Zn-Dio core. Compared with the uncoated Zn-Dio nanoparticles, the presence of the peripheral layer indicates modification of the nanoparticle surface following sequential coating with xylan and chitosan. The observed morphology provides additional morphological support for the proposed Zn-Dio-Xy/Chi nanostructure and complements the changes observed in particle size, zeta potential, and FTIR spectra.[24,25]

DSC analysis

The DSC thermogram of Dio exhibits two distinct sharp endothermic peaks, characteristic of a crystalline material, as shown in Figure 5A. The primary melting endotherm appears at 261.8 °C, confirming the high purity and thermal stability of the compound. In addition, a smaller endothermic peak is observed at 258.1 °C, which may be attributed to the presence of a polymorphic form or a pre-melting transition associated with structural rearrangement prior to complete melting.[26] The presence of well-defined melting peaks further supports the highly ordered crystalline structure of Dio.

The DSC thermogram of Zn reveals features typical of an amorphous material, including a glass transition temperature (Tg) around 182 °C. The absence of a distinct melting peak indicates a lack of long-range crystalline order within the protein matrix. A broad endothermic event at higher temperature may correspond to the onset of thermal degradation or minor structural transitions possibly associated with residual ordered regions within the protein structure.[27]

The thermogram of Xy displays a broad and intense endothermic peak, which is generally associated with thermal decomposition and the loss of bound or structural water molecules commonly present in polysaccharide systems. The absence of a well-defined melting peak further confirms the predominantly amorphous and polymeric nature of Xy, which is typical of natural polysaccharides due to their irregular chain arrangement and extensive intermolecular hydrogen bonding.[28]

Similarly, Chi exhibits a sharp endothermic peak around 313 °C, which is attributed to thermal decomposition of the polymer backbone. The absence of a distinct glass transition or melting peak suggests that Chi exists predominantly in an amorphous state. Its relatively high decomposition temperature indicates good thermal stability, making it suitable for use as a protective coating material in nanoparticle-based drug delivery systems.[29]

In the Zn-Dio nanoparticles, the characteristic sharp melting peak of Dio at approximately 257 °C is absent, and instead a broadened and slightly shifted thermal transition is observed. The disappearance of the drug's crystalline melting peak indicates that Dio is no longer present in its crystalline form but is likely molecularly dispersed within the Zn matrix. This behavior confirms successful encapsulation of the drug within the nanoparticle system. The relatively lower thermal stability of the uncoated Zn-Dio formulation compared with the coated system suggests that the polymeric coating provides additional thermal protection and structural reinforcement.

The DSC thermogram of the Zn-Dio-Xy/Chi nanoparticles further confirms successful drug encapsulation within the composite polymer matrix composed of Zn, Xy, and Chi. Notably, the sharp melting peak of pure Dio at approximately 257 °C is absent, indicating that the drug exists in an amorphous or molecularly dispersed state within the nanoparticle framework. The observed thermal profile suggests the presence of intermolecular interactions among Dio and the surrounding biopolymer matrix, which contribute to the stabilization of the amorphous form. Such amorphous dispersion is advantageous for drug delivery applications, as it can improve drug solubility, dissolution behavior, and controlled release characteristics of the nanoparticle system.

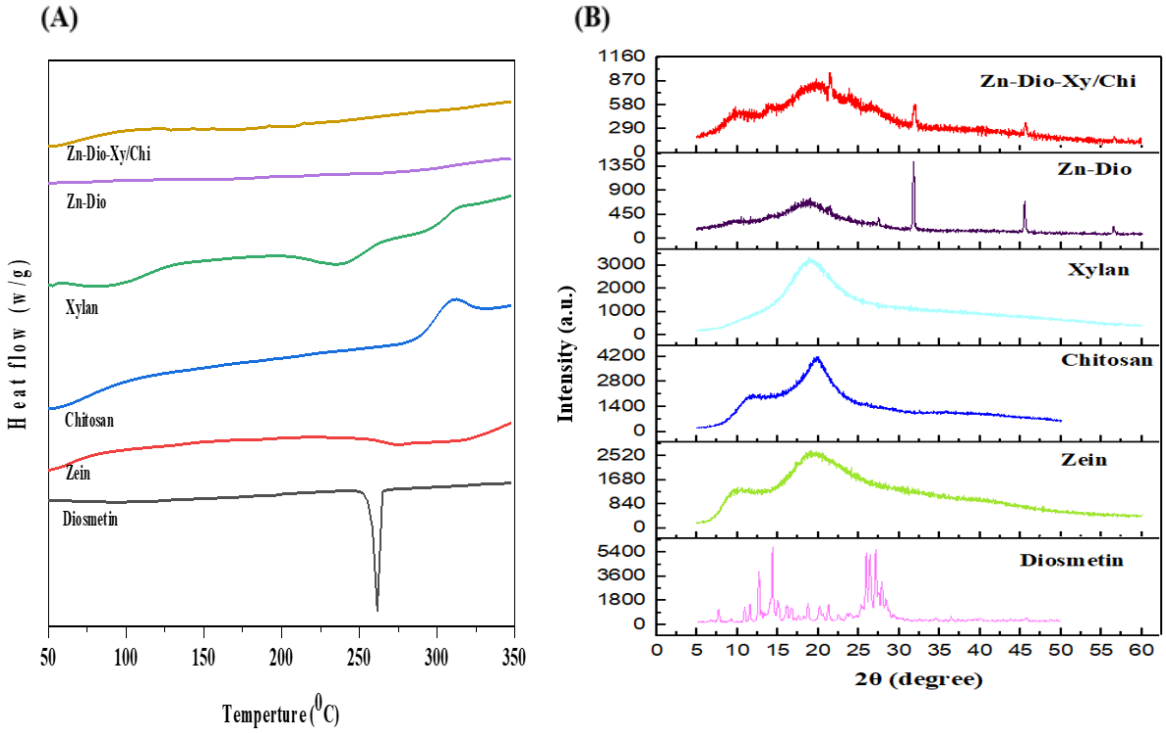


Figure 5: Thermograms (A) and diffractograms (B) of Dio, Xy, Zn, Zn-Dio, Chi and Zn-Dio-Xy/Chi nanoparticles

PXRD analysis

As illustrated in Figure 5B, the XRD pattern of pure Dio exhibits several sharp and intense diffraction peaks within the 2θ range of 5°–35°, confirming its highly crystalline nature. The pronounced peak intensities and narrow peak widths indicate a well-ordered molecular lattice structure. Such distinct reflections are characteristic of crystalline compounds and suggest strong intermolecular packing within the Dio structure. This high degree of crystallinity is commonly associated with limited aqueous solubility, thereby providing a strong rationale for employing nanoparticle-based strategies, such as amorphization or polymeric encapsulation, to enhance the dissolution behavior and bioavailability of Dio.[30]

The XRD profile of Zn shows a broad and diffuse peak centered around 2θ ≈ 20°, which is characteristic of an amorphous material. The absence of sharp diffraction peaks indicates a lack of long-range crystalline order, while the broad hump suggests the presence of short-range molecular organization typical of natural protein matrices. This predominantly amorphous structure is advantageous for drug delivery applications, as it facilitates improved molecular dispersion and can promote enhanced solubility of incorporated hydrophobic drugs. Consequently, the amorphous nature of Zn supports its role as an effective carrier matrix in nanoparticle systems designed to reduce the crystallinity of poorly water-soluble drugs such as Dio.[31]

Similarly, the XRD pattern of Xy reveals a broad peak centered around 2θ ≈ 20°, indicating its largely amorphous character. The absence of distinct sharp peaks suggests minimal crystalline domains, which is typical of many natural polysaccharides due to their irregular chain arrangements and extensive hydrogen bonding networks. A slight hump in the diffractogram indicates limited short-range molecular ordering, but no significant crystalline regions are observed. The amorphous structure of Xy is particularly beneficial in nanoparticle formulations, as it promotes uniform drug dispersion within the polymeric matrix and enhances the apparent solubility of poorly water-soluble drugs such as Dio.[32]

In the case of Chi, the XRD pattern displays a broad diffraction peak around 2θ ≈ 20°, indicating its semi-crystalline nature. While the presence of this peak suggests partial structural organization arising from intermolecular hydrogen bonding and chain alignment, the overall broadness and absence of sharp peaks indicate a substantial amorphous component. This semi-crystalline architecture is advantageous for polymeric coating applications,

as it provides a balance between structural integrity and flexibility, thereby supporting controlled drug release behavior in nanoparticle-based delivery systems.[33]

The diffractogram of Zn-Dio nanoparticles exhibits a broad halo in the region of $2\theta \approx 18°–22°$, suggesting that Dio is molecularly dispersed within the Zn matrix and has largely lost its original crystalline structure. Only minor peaks are observed at approximately $2\theta = 27°$, 32°, and 45°, and their relatively low intensity indicates that they do not correspond to significant crystalline domains of Dio. Notably, the characteristic sharp peaks associated with crystalline Dio are absent in the Zn-Dio formulation, confirming that the drug has undergone amorphization during the nanoparticle formation process. The predominance of an amorphous structure is advantageous for enhancing drug dissolution and solubility, thereby supporting the development of improved colon-targeted drug delivery systems with enhanced dissolution profiles and potentially higher bioavailability.

Furthermore, the XRD pattern of Zn-Dio-Xy/Chi nanoparticles displays broad and diffuse peaks within the 2θ range of approximately 18°–24°, indicating a further reduction in crystallinity. The absence of the characteristic crystalline peaks of Dio, particularly those observed near $2\theta \approx 12°$ and 27°, confirms that the drug remains molecularly dispersed within the polymeric matrix. The broad halo observed in the diffractogram indicates that the system predominantly exists in an amorphous state. The incorporation of Xy and Chi coatings appears to further suppress residual crystallinity, likely due to strong intermolecular interactions and the formation of a stabilizing polymeric network around the nanoparticle core.

The reduced peak intensity compared to the uncoated nanoparticles suggests improved encapsulation efficiency and more effective stabilization of the amorphous drug form. Additionally, the presence of Xy and Chi coatings is expected to enhance mucoadhesive properties and provide protection of the nanoparticle system during gastrointestinal transit. Overall, the XRD results confirm that the Zn-Dio-Xy/Chi nanoparticle system exhibits a predominantly amorphous structure, indicating successful drug encapsulation and molecular dispersion. This structural transformation is expected to contribute to enhanced solubility, improved formulation stability, and efficient colon-targeted drug delivery.

FTIR analysis

The FTIR spectra of the individual components and nanoparticle formulations are presented in Figure 6. The spectrum of Dio exhibited several characteristic absorption bands corresponding to its phenolic and aromatic functional groups. A broad band observed in the range of 3744–3401 cm^{-1} was attributed to O–H stretching vibrations of phenolic hydroxyl groups, which are typical structural features of flavonoids. A distinct absorption band at approximately 1745 cm^{-1} corresponds to the C=O stretching vibration of an ester or conjugated carbonyl group. Additionally, peaks within the 1660–1600 cm^{-1} region are associated with C=C stretching vibrations of aromatic rings, while the bands appearing between 1160 and 1020 cm^{-1} correspond to C–O stretching vibrations of phenolic and alcoholic groups. These characteristic peaks confirm the chemical structure of Dio and its functional groups involved in potential intermolecular interactions within the nanoparticle system.[34]

The FTIR spectrum of Xy displayed a broad and intense absorption band at approximately 3419 cm^{-1}, which corresponds to O–H stretching vibrations of hydrogen-bonded hydroxyl groups, a common feature of polysaccharide structures. Peaks observed in the 2914–2931 cm^{-1} range were attributed to aliphatic C–H stretching vibrations of the sugar backbone. Furthermore, a strong absorption band between 1043 and 1064 cm^{-1} was assigned to C–O–C stretching vibrations associated with glycosidic linkages and ether bonds within the Xy polysaccharide framework. These spectral features confirm the typical polysaccharide structure of Xy and its suitability as a biopolymer for nanoparticle coating.[35-37]

The FTIR spectrum of Zn exhibited characteristic protein-related absorption bands, including N–H stretching around 3300 cm^{-1}, amide I absorption near 1655 cm^{-1}, and amide II bands around 1540 cm^{-1}, confirming the presence of a proteinaceous structure. Additional peaks corresponding to C–H and C–O stretching vibrations indicate the presence of alkyl side chains and minor carbohydrate residues associated with the protein matrix. These spectral features are consistent with the typical structural characteristics of Zn and support its role as a protein-based carrier material for drug encapsulation.[38]

The FTIR spectrum of Chi displayed characteristic absorption bands at 3363 and 3285 cm^{-1}, corresponding to –OH and $–NH_2$ stretching vibrations, respectively. Additional peaks at 1150

cm^{-1} and 1020 cm^{-1} were attributed to C–O–C stretching vibrations associated with the polysaccharide backbone. These absorption bands confirm the presence of the essential functional groups of Chi and demonstrate the structural integrity of the polymer, supporting its suitability as a biopolymer coating material in nanoparticle-based drug delivery systems.[39]

The FTIR spectrum of the Zn-Dio nanoparticles exhibited characteristic absorption bands associated with the functional groups of Zn and Dio. A broad absorption band in the region of 3300-3400 cm^{-1} was attributed to O–H stretching of Dio and N–H stretching of the Zn protein. The bands around 2920-2960 cm^{-1} correspond to aliphatic C–H stretching vibrations. A prominent band at approximately 1641 cm^{-1} can be assigned mainly to the amide I (C=O stretching) vibration of Zn, with possible contribution from the conjugated carbonyl group of Dio. The band in the region of 1530 cm^{-1} is characteristic of the amide II vibration of Zn, arising predominantly from N–H bending coupled with C–N stretching. The absorption bands in the 1323–1170 cm^{-1} region can be associated with C–O, C–C and C–N stretching vibrations, reflecting the functional groups present in Dio and Zn. The band around 1040-1151 cm^{-1} may be related to C–O/C–C stretching vibrations. Additional fingerprint-region bands around 980–713 cm^{-1} may be attributed to aromatic C–H out-of-plane and skeletal vibrations of Dio. The characteristic functional groups of Zn and Dio were retained in the Zn-Dio nanoparticles, while changes in relative intensity and/or band position compared with the individual components indicate molecular interactions between Dio and Zn during nanoparticle formation.[40,41]

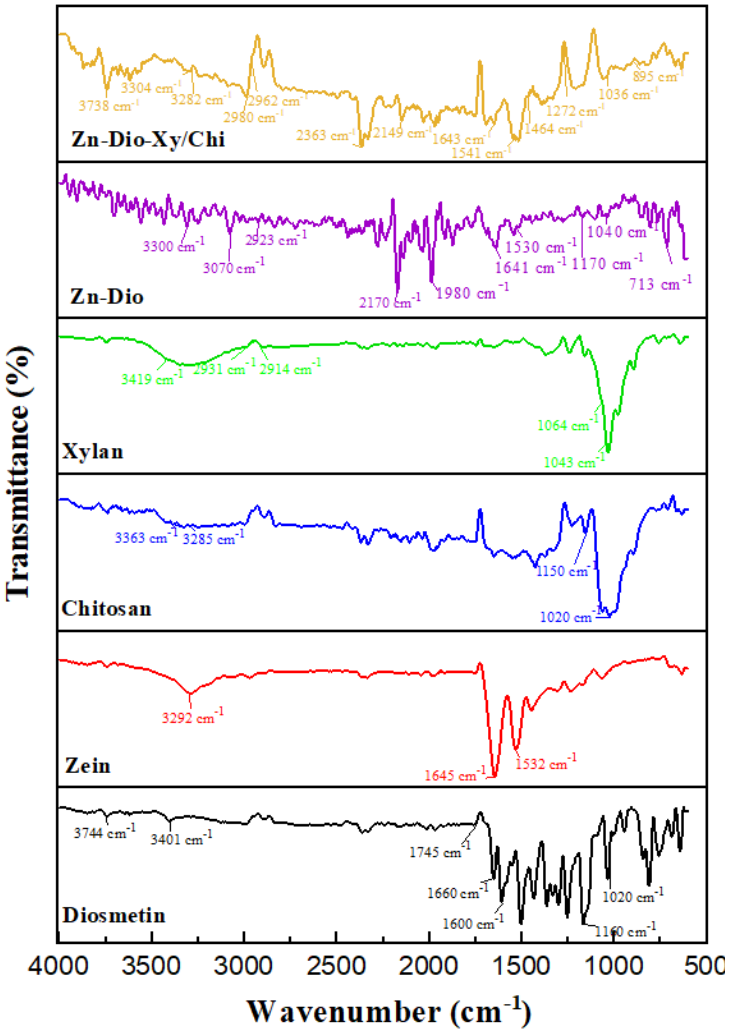


Figure 6: FTIR spectra of Dio, Xy, Zn, Zn-Dio, Chi and Zn-Dio-Xy/Chi nanoparticles

The FTIR spectrum of the Zn-Dio-Xy/Chi nanoparticles showed characteristic absorption bands corresponding to the functional groups of Zn, Dio, Xy, and Chi, with changes in band intensity and position after nanoparticle formation. A broad absorption region at approximately 3282–3304 cm^{-1} can be attributed mainly to O–H and N–H stretching vibrations, originating from the hydroxyl groups of Xy/Chi and the amide groups of Zn. The band observed around 2963 cm^{-1} corresponds to aliphatic C–H stretching vibrations. A prominent band around 1643 cm^{-1} can be associated with amide I (C=O stretching) of Zn, together with the conjugated carbonyl vibration of Dio and the contribution of Chi/Xy functional groups. The absorption band near 1541 cm^{-1} is characteristic of amide II vibrations (N–H bending coupled with C–N stretching) of the protein component and may also overlap with aromatic skeletal vibrations of Dio. The bands in the 1464–1427 cm^{-1} region are attributable to C–H bending and/or O–H deformation vibrations, while the fingerprint-region absorption around 1280–1260 cm^{-1} may arise from C–O stretching, C–N stretching and polysaccharide-related vibrations. A strong band at approximately 1036 cm^{-1} is particularly relevant to the polysaccharide coating and can be assigned to C–O–C/C–O stretching vibrations of Xy and Chi. The band around 895 cm^{-1} can be associated with glycosidic-linkage/polysaccharide skeletal vibrations, supporting the presence of the carbohydrate components. The characteristic bands of the individual components were retained, although changes in intensity and slight shifts/broadening were observed in the nanoparticle spectrum, suggesting intermolecular interactions among Zn, Dio, Xy and Chi during nanoparticle formation rather than the formation of entirely new covalent functional groups.

The coexistence of these characteristic peaks confirms the successful encapsulation of Dio within the Zn matrix and effective surface coating with Chi and Xy polymers. The slight peak shifts and band broadening suggest the presence of hydrogen bonding and electrostatic interactions among Zn, Dio, Xy, and Chi, which contribute to the structural stability of the nanoparticle system. The FTIR results demonstrate the successful formation of a multi-component nanoparticle system stabilized through non-covalent interactions. The presence of Xy and Chi coatings may further contribute to pH-responsive behavior and enzymatic biodegradability in the colon, supporting the suitability of this formulation as a colon-targeted drug delivery system.[42]

Stability evaluation

Thermal stability

The effect of temperature on the particle size of the nanoparticle formulations is illustrated in Figure 7A. The Zn-Dio nanoparticles exhibited a gradual increase in particle size with rising temperature. Specifically, the particle sizes were measured as 350.4 ± 0.25 nm, 356.18 ± 0.41 nm, 358.02 ± 0.15 nm, 360.81 ± 0.35 nm, 364.82 ± 0.11 nm, and 367.01 ± 0.44 nm at 40, 50, 60, 70, 80, and 90 °C, respectively. This progressive increase indicates that the particle size of the Zn-Dio formulation is temperature dependent, likely due to enhanced molecular mobility and partial destabilization of the nanoparticle interface at elevated temperatures. Increased thermal energy may weaken intermolecular interactions within the nanoparticle matrix, leading to slight aggregation or expansion of the nanoparticle structure, thereby contributing to the observed size increase.

In contrast, the Zn-Dio-Xy/Chi nanoparticles demonstrated relatively stable particle sizes across the same temperature range. The recorded values were 548.02 ± 0.09 nm, 546.52 ± 0.25 nm, 544.42 ± 0.31 nm, 547.46 ± 0.07 nm, 550.10 ± 0.20 nm, and 551.12 ± 0.09 nm at 40, 50, 60, 70, 80, and 90 °C, respectively. The minimal variation in particle size indicates that the Xy/Chi coating provides a protective stabilizing layer, effectively preserving nanoparticle integrity under thermal stress. The polysaccharide coating likely forms a barrier that restricts particle aggregation and structural rearrangement, thereby maintaining a stable hydrodynamic diameter even at elevated temperatures.

A similar stability trend was observed in the zeta potential measurements, as presented in Figure 7B. The zeta potential of the Zn-Dio-Xy/Chi nanoparticles remained nearly constant throughout the temperature range, varying only slightly from +41.10 ± 0.20 mV to +40.14 ± 0.08 mV. In comparison, the Zn-Dio nanoparticles exhibited a slight variation in surface charge, with zeta potential values ranging between −21.25 ± 0.58 mV and −20.52 ± 0.50 mV. Although these changes were relatively small, they indicate a comparatively lower resistance of the uncoated nanoparticles to temperature-induced alterations in surface properties.

The consistent zeta potential values observed for the coated nanoparticles further confirm their

excellent colloidal stability under elevated temperature conditions. This enhanced stability can be attributed to strong intermolecular interactions, including hydrogen bonding and hydrophobic interactions among the Zn, Xy, and Chi components, which collectively reinforce the nanoparticle structure and reduce the likelihood of particle aggregation.

Overall, these findings demonstrate that the Zn-Dio-Xy/Chi nanoparticle system exhibits superior thermal stability compared to the uncoated Zn-Dio formulation. The presence of the Xy/Chi coating plays a crucial role in maintaining nanoparticle size and surface charge stability under thermal stress, highlighting its importance in improving the robustness and reliability of the nanoparticle system for drug delivery applications.[4]

Ionic strength stability

The stability of the prepared nanoparticles under varying ionic strength was evaluated by monitoring changes in particle size and zeta potential following the addition of increasing concentrations of NaCl (0–200 mM). Variations in electrolyte concentration are known to influence colloidal stability because the ionic strength affects the thickness of the electrical double layer surrounding nanoparticles, thereby altering interparticle interactions and aggregation behavior.[43,44] The corresponding results are presented in Figure 7C–D.

For the Zn-Dio nanoparticles, a pronounced increase in particle size was observed with increasing NaCl concentration. The particle size increased from 350.4 ± 0.5 nm at 0 mM to 380.85 ± 0.39 nm, 722.04 ± 1.65 nm, 1112.20 ± 3.39 nm, 1536.21 ± 1.24 nm, and 1820.0 ± 22 nm at 10, 20, 50, 100, and 200 mM NaCl, respectively. Concurrently, the zeta potential became less negative, shifting from −21.25 ± 0.01 mV to −2.60 ± 0.15 mV with increasing salt concentration. This progressive reduction in surface charge with rising ionic strength is consistent with classical DLVO theory, which predicts that electrolytes compress the electrical double layer surrounding charged particles, thereby reducing electrostatic repulsion and promoting aggregation.[45,46]

The pronounced salt sensitivity of the Zn-Dio nanoparticles can be attributed to charge screening effects caused by Na^+ ions. As Na^+ ions interact with the negatively charged nanoparticle surface, the magnitude of the surface charge is reduced. This reduction in electrostatic repulsion allows van der Waals attractive forces to dominate, facilitating particle–particle interactions and resulting in aggregation. Consequently, a substantial increase in particle size was observed at higher ionic strengths.

In contrast, the Zn-Dio-Xy/Chi nanoparticles exhibited remarkable resistance to salt-induced destabilization. The particle size remained relatively stable across the entire ionic strength range, with values of 547.5 ± 0.65 nm, 548.2 ± 0.45 nm, 550.25 ± 0.04 nm, 551.04 ± 0.04 nm, 554.2 ± 0.21 nm, and 557.30 ± 12 nm at 0–200 mM NaCl, respectively. Similarly, the zeta potential showed only a minor decrease, changing from +41.10 ± 0.07 mV to +38.01 ± 0.01 mV.[47,48]

The enhanced stability of the Xy/Chi-coated nanoparticles can be attributed to the combined effects of steric stabilization and residual electrostatic repulsion. The polysaccharide coating forms a hydrated steric barrier around the nanoparticle surface, which restricts close particle–particle contact and prevents aggregation even under conditions of high ionic strength. In addition, the retained positive surface charge contributes to electrostatic repulsion between particles, further enhancing colloidal stability.

Collectively, these findings demonstrate that the Xy/Chi coating significantly improves the salt tolerance and colloidal stability of the nanoparticle system, ensuring structural integrity under physiological ionic conditions. Such stability is particularly advantageous for oral and colon-targeted drug delivery applications, where nanoparticles are exposed to complex electrolyte environments within the gastrointestinal tract.[49]

pH Stability

The pH-dependent stability of the Zn-Dio-Xy/Chi nanoparticles was evaluated across a pH range of 4.0-8.0, and the corresponding results are presented in Figure 7E–F. As shown in Figure 7E, the particle size of the Zn-Dio-Xy/Chi nanoparticles exhibited only minor variations throughout the tested pH range. The measured particle sizes were 548.2 ± 0.14 nm, 550.21 ± 0.31 nm, 560.71 ± 0.44 nm, 564.38 ± 0.30 nm, and 569.52 ± 0.22 nm at pH 4, 5, 6, 7, and 8, respectively. These minimal changes indicate that the particle size of the coated nanoparticles remains largely unaffected by pH variations, suggesting strong structural stability of the formulation under different environmental conditions.

In contrast, the Zn-Dio nanoparticles displayed a noticeable reduction in zeta potential, reaching

approximately −15 ± 0.01 mV near the isoelectric point of zein (around pH 6), as illustrated in Figure 7F. At or near the isoelectric point, the net surface charge of the nanoparticles decreases due to the balance between positive and negative charges on the protein molecules. This reduction in surface charge leads to weaker electrostatic repulsion between particles, thereby increasing the likelihood of particle aggregation and reducing overall colloidal stability.

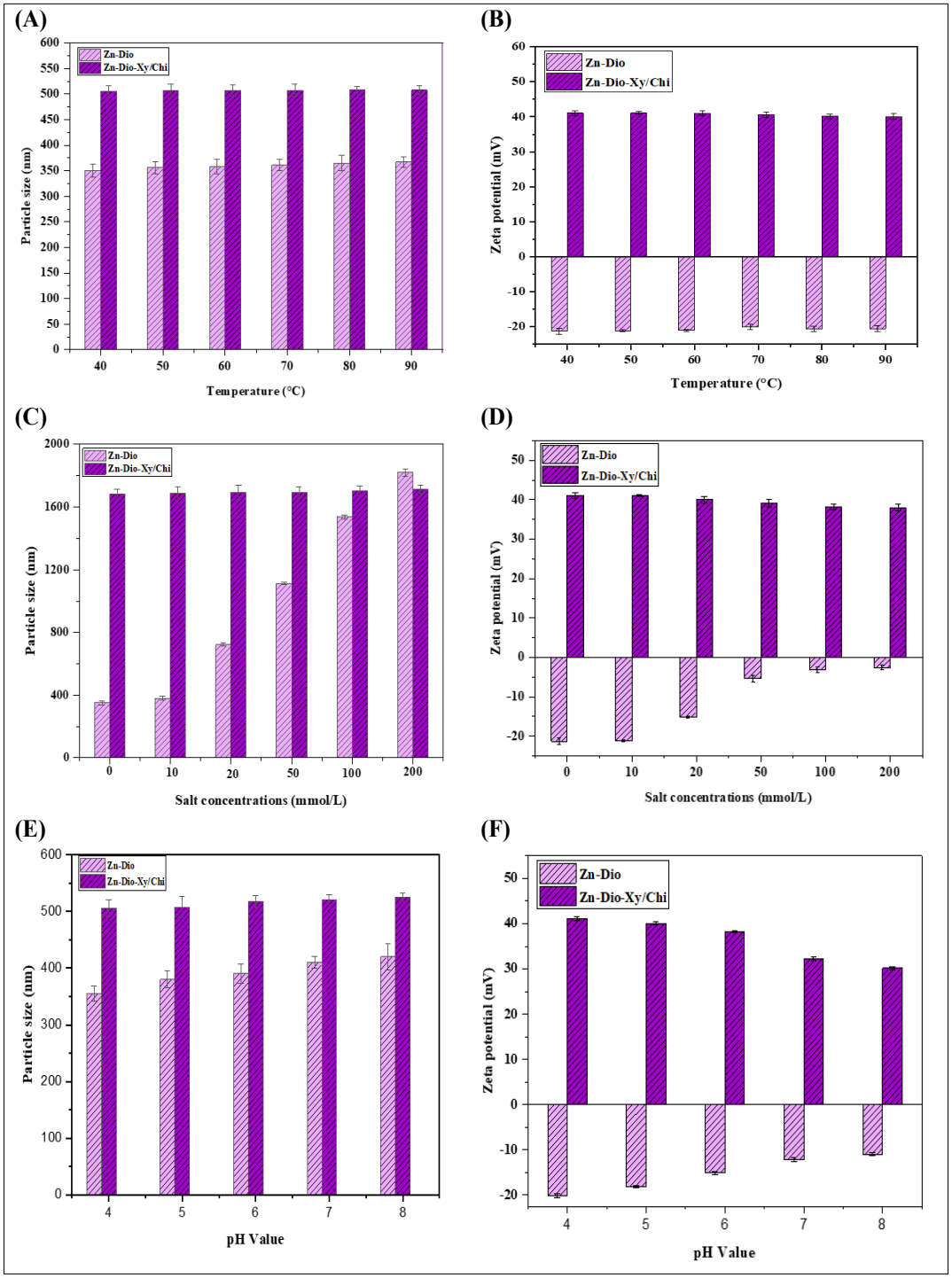


Figure 7: Thermal stability of Zn-Dio and Zn-Dio-Xy/Chi: (A) Particle size, and (B) Zeta-potential; Ionic stability of Zn-Dio and Zn-Dio-Xy/Chi: (C) Particle size, (D) Zeta-potential; pH stability of Zn-Dio and Zn-Dio-Xy/Chi: (E) Particle size and (F) Zeta-potential

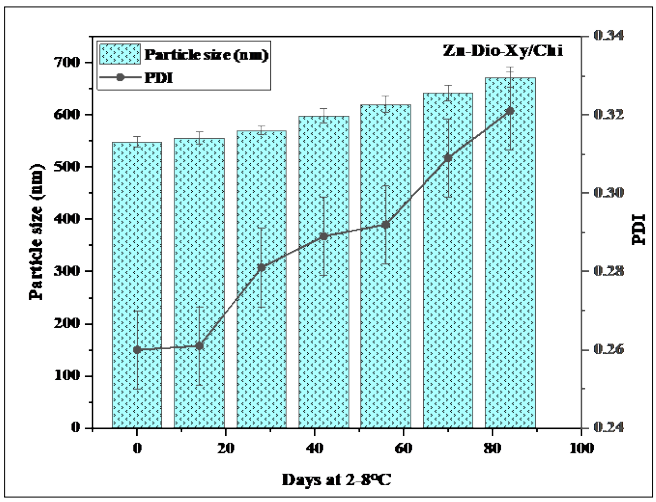


Figure 8: Storage stability of Zn-Dio-Xy/Chi

Conversely, the Zn-Dio-Xy/Chi nanoparticles maintained relatively stable particle size and zeta potential values across the entire pH range, confirming the stabilizing effect of the Xy and Chi coatings. The presence of these biopolymers provides both electrostatic and steric stabilization, which helps to preserve nanoparticle integrity under varying pH conditions. The polysaccharide coating likely forms a protective hydrated layer around the nanoparticles, where hydrogen bonding interactions and electrostatic forces contribute to maintaining particle separation and preventing aggregation even under mildly acidic conditions.

Overall, these results demonstrate that the Xy/Chi coating significantly enhances the colloidal and electrostatic stability of Zn-Dio nanoparticles across a broad pH range. Such stability is particularly important for oral and colon-targeted drug delivery systems, where nanoparticles must withstand the dynamic pH conditions encountered along the gastrointestinal tract. The improved pH stability therefore supports the potential application of the Zn-Dio-Xy/Chi nanoparticle system for efficient and reliable drug delivery.[50]

Storage stability

The long-term storage stability of the Zn-Dio-Xy/Chi nanoparticles was evaluated over a period of 90 days at 2–8 °C, and the results are presented in Figure 8. As shown in the figure, the particle size remained relatively stable throughout the storage period, indicating good physical stability of the nanoparticle formulation. The measured particle sizes were 548.20 ± 0.01 nm, 555.22 ± 0.35 nm, 570.32 ± 0.12 nm, 598.11 ± 0.45 nm, and 620.17 ± 0.38 nm on days 0, 14, 30, 60, and 90, respectively.

The slight increase in particle size over time may be attributed to minor nanoparticle aggregation or gradual hydration and swelling of the polysaccharide coating layer, phenomena that are commonly observed in biopolymer-based nanoparticle systems during prolonged storage. Such changes are generally minimal and do not significantly affect the overall structural integrity of the formulation, which is consistent with findings reported in previous nanoparticle stability studies.

The PDI values exhibited only a small increase, rising from 0.260 ± 0.12 to 0.292 ± 0.01 over the storage period. Importantly, the PDI values remained below 0.3, indicating that the nanoparticle system maintained a relatively narrow and uniform size distribution, which is a key indicator of good colloidal stability in nanoparticle formulations.

Furthermore, the zeta potential values remained nearly constant during the entire storage period, suggesting that the Xy/Chi coating effectively preserved the surface charge of the nanoparticles and prevented significant particle aggregation. The maintenance of a stable surface charge is essential for sustaining electrostatic repulsion between particles and ensuring long-term colloidal stability.

Overall, these results demonstrate that the Zn-Dio-Xy/Chi nanoparticles retained good structural integrity and colloidal stability during 90 days of refrigerated storage, highlighting the stabilizing role of the Xy/Chi biopolymeric coating. The observed stability supports the potential suitability

of this nanoparticle system for long-term therapeutic and drug delivery applications.[50]

Simulated gastrointestinal digestion

Figure 9 illustrates the simulated gastrointestinal release profile of Dio from Zn-Dio and Zn-Dio-Xy/Chi nanoparticles under sequential gastrointestinal conditions. The results clearly demonstrate that both encapsulation within the Zn matrix and subsequent Xy/Chi coating significantly influence the release behavior of Dio under different physiological environments.

In simulated gastric fluid (SGF, pH 1.2), the Zn-Dio formulation released 12.31 ± 0.03% of Dio within the first 2 h, whereas the coated Zn-Dio-Xy/Chi nanoparticles released only 9.303 ± 0.04% during the same period. The comparatively lower drug release in acidic conditions indicates that the Xy/Chi coating effectively protects the nanoparticles from premature drug release in the gastric environment. This protective effect can be attributed primarily to the protonation of chitosan (Chi) under acidic conditions, which promotes the formation of a compact and less permeable polymeric layer around the nanoparticle surface, thereby restricting the diffusion of Dio from the matrix.

Upon transition to simulated intestinal fluid (SIF, pH 6.8), a gradual increase in drug release was observed. The cumulative release of Dio from Zn-Dio nanoparticles reached 42.20 ± 0.04% after 6 h, whereas the Zn-Dio-Xy/Chi nanoparticles exhibited a slower and more controlled release of 29.25 ± 0.02%. This moderate increase in drug release suggests that partial swelling of the polymeric coating and ion-exchange processes within the matrix enhanced the diffusion of Dio without causing complete structural disintegration of the nanoparticles. The comparatively lower release rate from the coated nanoparticles indicates that the Xy/Chi layer effectively regulates drug diffusion under near-neutral pH conditions.

In simulated colonic fluid (SCF, pH 7.4), a substantial increase in drug release was observed. The Zn-Dio nanoparticles released 85.59 ± 0.04% of Dio after 24 h, indicating extensive diffusion of the drug from the Zn matrix once the surrounding environment approached neutral to slightly alkaline conditions. In contrast, the Zn-Dio-Xy/Chi nanoparticles exhibited a more sustained release profile, reaching 63.19 ± 0.05% over the same period. The slower release from the coated nanoparticles is attributed to the enzymatic degradation of Xy by colonic microflora-simulating enzymes, which gradually breaks down the polysaccharide coating and enables controlled release of Dio at the target site. This enzyme-responsive degradation mechanism ensures that the majority of drug release occurs in the colonic environment, which aligns with the objectives of colon-targeted drug delivery.[51]

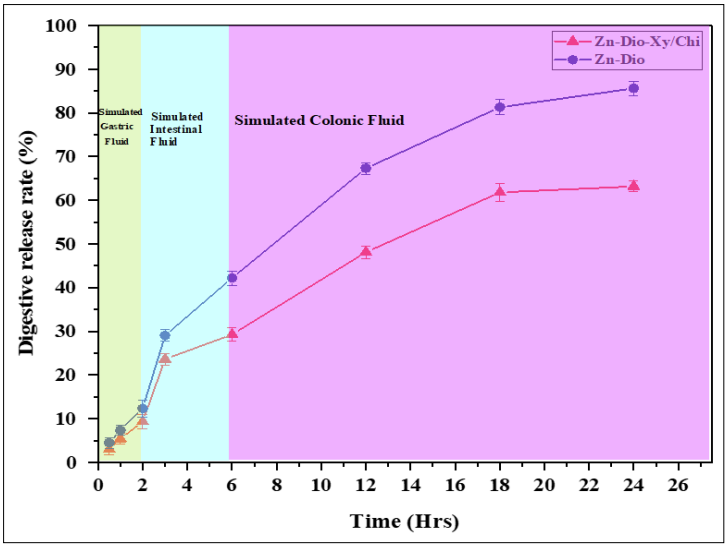


Figure 9: Simulated gastrointestinal digestion of Dio from Zn-Dio-Xy/Chi and Zn-Dio

Table 1
Kinetic models for Zn-Dio-Xy/Chi

Kinetic models	k	n	R^2	Release mechanism
Zero-order	2.6814	N/A	0.9185	Constant-rate release
First-order	0.0192	N/A	0.9601	Concentration-dependent release
Higuchi	15.637	N/A	0.9782	Diffusion-controlled
Korsmeyer–Peppas	6.00	0.8177	0.9634	Anomalous/non-Fickian transport

Overall, the sequential release trend observed across the simulated gastrointestinal media (SGF < SIF < SCF) confirms that the Xy/Chi dual coating provides staged protection and controlled drug release. The coating minimizes premature drug loss in the upper gastrointestinal tract while promoting enhanced release in the colonic region. This behavior can be explained by the pH-sensitive solubility of Chi and the microbial degradability of Xy, which together provide complementary chemical (pH-dependent) and biological (enzyme-triggered) stimuli for controlled drug release. The simulated gastrointestinal digestion study therefore demonstrates that the Xy/Chi coating significantly improves nanoparticle stability under gastric and intestinal conditions while enabling sustained and enzyme-responsive release in the colon. Consequently, this dual-functional coating system represents a promising platform for the colon-targeted delivery of poorly soluble flavonoids such as Dio, potentially improving their local bioavailability and therapeutic efficacy in colonic disorders.

To further elucidate the drug release mechanism, the drug-release data were fitted to zero-order, first-order, Higuchi, and Korsmeyer–Peppas kinetic models. The corresponding kinetic parameters, including the release-rate constant (k), release exponent (n), and coefficient of determination (R^2), are presented in Table 1. The Higuchi model exhibited the highest correlation coefficient ($R^2 = 0.9782$), indicating that diffusion was the predominant process governing drug release from the nanoparticulate system. Furthermore, analysis using the Korsmeyer-Peppas model yielded an n value of 0.8177 ($R^2 = 0.9634$). The n value between 0.43 and 0.85 indicates anomalous (non-Fickian) transport, suggesting that drug release involves a combination of diffusion and polymer relaxation/erosion. Thus, the release behavior can be described as predominantly diffusion-controlled, with a contribution from polymer relaxation/erosion.

The hydrophilic nature of the xylan–chitosan coating forms a diffusion-regulating barrier that slows drug migration and enables sustained release over 24 h. Collectively, these kinetic results confirm that the Zn-Dio-Xy/Chi nanoparticle system exhibits controlled and diffusion-dominated drug release behavior, which is highly suitable for colon-targeted drug delivery applications.

CONCLUSION

This study addressed diosmetin's poor aqueous solubility and low oral bioavailability by designing a colon-targeted nanocarrier based on a hydrophobic zein core coated with xylan (microbiota-degradable) and chitosan (mucoadhesive) to achieve pH- and enzyme-responsive release for colon disorders. Diosmetin-loaded zein nanoparticles were prepared via antisolvent nanoprecipitation and coated with xylan and chitosan solutions, followed by optimization using particle size/PDI, zeta potential, encapsulation efficiency, and loading capacity. Characterization showed coating increased particle size and reversed surface charge: zein 180.1 nm (PDI 0.18), zein-diosmetin 350.4 nm (PDI 0.23; zeta -21.25 mV), and coated formulations 548-920 nm (PDI 0.26-0.29), with optimized Zn:Dio:Xy:Chi ratio of 1:1:1 yielding 548 nm, PDI 0.26, and zeta +41.10 mV. Encapsulation efficiency improved from 85.0% to 92.82% with coating, while loading capacity decreased from 22.08% to 9.28%; SEM confirmed spherical particles with coated architecture. Solid-state analyses indicated successful encapsulation without diosmetin degradation, showing amorphization within the matrix and improved thermal protection up to 215 °C. The xylan/chitosan shell enhanced stability under thermal stress, ionic strength, pH variation, and storage conditions. *In vitro* digestion demonstrated

effective upper-GIT protection and colon-favored release: coated nanoparticles released 9.30% in gastric fluid, 29.25% in intestinal fluid, and 63.19% in colonic fluid with enzymes over 24 h, supporting pH sensitivity and enzyme-triggered release; kinetics followed the Higuchi model (R^2=0.9782). The work shows xylan–chitosan coated zein nanocarriers can overcome diosmetin's solubility constraints while providing stable, enzyme-responsive, colon-targeted delivery for potential colorectal cancer therapy applications.

ACKNOWLEDGMENT: The authors extend their gratitude to the Management and Principal of H. R. Patel Institute of Pharmaceutical Education and Research for providing the necessary facilities for the successful completion of this research.

REFERENCES

[1] M. Garg, S. Chaudhary, A. Goyal, P. Sarup, S. Kumari *et al*., *Phytomed. Plus*, **2**, 100179 (2022), https://doi.org/10.1016/j.phyplu.2021.100179
[2] M. Wujec and M. Feldo, *Molecules*, **28**, 7910 (2023), https://doi.org/10.3390/molecules28237910
[3] W. X. Sun, C. T. Zhang, X. Yu, J. Guo, H. Ma *et al*., *J. Funct. Foods*, **91**, 105027 (2022), https://doi.org/10.1016/j.jff.2022.105027
[4] S. Jadhav, S. Nangare, P. Bafna, P. Baviskar and L. Zawar, *Cellulose Chem. Technol*., **59**, 789 (2025), https://doi.org/10.35812/CelluloseChemTechnol.2025.59.67
[5] Y. Anda-Flores, E. Carvajal-Millan, A. Campa-Mada, J. Lizardi-Mendoza, A. Rascon-Chu *et al*., *Polysaccharides*, **2**, 626 (2021), https://doi.org/10.3390/polysaccharides2030038
[6] L. Campos, A. Neto, M. Noronha, M. Lima, I. Cavalcanti *et al*., *Int. J. Pharm*., **635**, 122754 (2023), https://doi.org/10.1016/j.ijpharm.2023.122754
[7] L. Campos, A. Neto, A. Scavuzzi, A. Lopes, N. Santos-Magalhães *et al*., *Pharmaceuticals*, **17**, 320 (2024), https://doi.org/10.3390/ph17030320
[8] H. Choukaife, S. Seyam, B. Alallam, A. A. Doolaanea and M. Alfatama, *Int. J. Nanomed*., **17**, 3933 (2022), https://doi.org/10.2147/IJN.S375229
[9] N. Zeybek, A. Buyukkileci, S. Gulec, M. Polat and H. Polat, *J. Drug Deliv. Sci. Technol*., **79**, 103983 (2023), https://doi.org/10.1016/j.jddst.2022.103983
[10] S. Lee, R. Bajracharya, J. Min, J. Han, B. J. Park *et al*., *Pharmaceutics*, **12**, 68 (2020), https://doi.org/10.3390/pharmaceutics12010068
[11] C. Yu, J. Shan, Z. Fu, H. Ju, X. Chen *et al*., *Foods*, **12**, 2861 (2023), https://doi.org/10.3390/foods12152861
[12] M. Wang, Y. Fu, Y. Shi, G. Chen, X. Li *et al*., *Food Hydrocoll*., **77**, 577 (2017), https://doi.org/10.1016/j.foodhyd.2017.10.036
[13] T. Mosmann, *J. Immunol. Methods*, **65**, 55 (1983)
[14] M. Hansen, S. Nielsen and K. Berg, *J. Immunol. Methods*, **119**, 203 (1989)
[15] C. Gonzalez, D. González, R. N. Zúñiga, H. Estay and E. Troncoso, *Foods*, **9**, 913 (2020), https://doi.org/10.3390/foods9070913
[16] D. Yadav and N. Kumar, *Int. J. Pharm*., **477**, 564 (2014), https://doi.org/10.1016/j.ijpharm.2014.10.070
[17] Sauraj, S. Kumar, V. Kumar, R. Priyadarshi, P. Gopinath *et al*., *Carbohydr. Polym*., **188**, 252 (2018), https://doi.org/10.1016/j.carbpol.2018.02.006
[18] Y. Luo and Q. Wang, *Int. J. Biol. Macromol*., **64**, 353 (2013), https://doi.org/10.1016/j.ijbiomac.2013.12.017
[19] R. Hogg, *KONA Powder Part. J*., **30** (2013)
[20] X. Jiang, Y. Li, X. Tang, J. Jiang, Q. He *et al*., *Environ. Sci. Pollut. Res*., **28**, 46934 (2021), https://doi.org/10.1007/s11356-021-15299-y
[21] M. Li and M. Yu, *J. Food Sci*., **85**, 4108 (2020), https://doi.org/10.1111/1750-3841.15535
[22] E. Oleandro, M. Stanzione, G. Buonocore and M. Lavorgna, *Nanomaterials*, **14**, 414 (2024), https://doi.org/10.3390/nano14050414
[23] H. H. Farghal, M. Nebsen and M. M. H. El-Sayed, *Water*, **15**, 829 (2023), https://doi.org/10.3390/w15040829
[24] Z. Lin, L. Zhan, K. Qin, Y. Li, Y. Qin *et al*., *Foods*, **13**, 1837 (2024), https://doi.org/10.3390/foods13121837
[25] V. Tkachenko, L. Vidal, L. Josien, M. Schmutz, J. Poly *et al*., *Polymers*, **12**, 1656 (2020), https://doi.org/10.3390/polym12081656
[26] Z. Gu, Y. Xue, S. Li, M. Adu-Frimpong, Y. Xu *et al*., *AAPS PharmSciTech*, **23**, 106 (2022), https://doi.org/10.1208/s12249-022-02263-3
[27] E. Corradini, P. S. Curti, A. B. Meniqueti, A. F. Martins, A. F. Rubira *et al*., *Int. J. Mol. Sci*., **15**, 22438 (2014), https://doi.org/10.3390/ijms151222438
[28] H. Marcelino, A. E. da Silva, M. Salgado Gomes, E. Oliveira, T. Nagashima-Junior *et al*., *Polymers*, **7**, 2304 (2015), https://doi.org/10.3390/polym7111515
[29] S. N. Ghanem, M. I. Marzouk, M. E. Tawfik and S. B. Eskander, *BMC Chem*., **19**, 214 (2025), https://doi.org/10.1186/s13065-025-01558-3
[30] Y. Zhang and K. Brad, *Appl. Mech. Mater*., **295–298**, 298 (2013), https://doi.org/10.4028/www.scientific.net/AMM.295-298.298
[31] G. Liu, D. An, J. Li and S. Deng, *Front. Pharmacol*., **14**, 1120251 (2023), https://doi.org/10.3389/fphar.2023.1120251
[32] N. Sobri, S. Harun, J. Jahim, M. Masdar, M. Takriff *et al*., *BioResources*, **18**, 1525 (2023), https://doi.org/10.15376/biores.18.1.1525-1544
[33] E. Alehosseini, H. Tabarestani, M. Kharazmi and S. Jafari, *Foods*, **11**, 3841 (2022), https://doi.org/10.3390/foods11233841
[34] H. Angamuthu and M. Ramachandrane, *J. Mol. Recognit*., **33**, e2819 (2019), https://doi.org/10.1002/jmr.2819

[35] K. Sharma, K. Khaire, A. Thakur, V. Moholkar and A. Goyal, *ACS Omega*, **5**, 13729 (2020), https://doi.org/10.1021/acsomega.0c00896
[36] G. Xu, W. Kong, C. Liu, R. Sun and J. Ren, *Materials*, **10**, 971 (2017), https://doi.org/10.3390/ma10080971
[37] F. Dai, Q. Zhuang, G. Huang, H. Deng and X. Zhang, *ACS Omega*, **8**, 17064 (2023), https://doi.org/10.1021/acsomega.3c01336
[38] R. Paliwal and S. Palakurthi, *J. Control. Release*, **189**, 108 (2014), https://doi.org/10.1016/j.jconrel.2014.06.036
[39] J. Kumirska, M. Czerwicka, Z. Kaczyński, A. Bychowska, K. Brzozowski *et al*., *Mar. Drugs*, **8**, 1567 (2010), https://doi.org/10.3390/md8051567
[40] R. Shukla and M. Cheryan, *Ind. Crop. Prod*., **13**, 171 (2001)
[41] A. Patel and K. P. Velikov, *Curr. Opin. Colloid Interface Sci*., **19**, 450 (2014), https://doi.org/10.1016/j.cocis.2014.08.001
[42] R. Zara, P. Bittencourt, T. Tiuman, V. Galan, F. de Souza *et al*., *J. Appl. Pharm. Sci*., **11**, 089 (2021), https://doi.org/10.7324/JAPS.2021.110709
[43] S. Bhattacharjee, *J. Control. Release*, **235**, 337 (2016), https://doi.org/10.1016/j.jconrel.2016.06.017
[44] R. J. Hunter, *Colloids Surf. A*, **210**, 125 (2002)
[45] B. Derjaguin and L. Landau, *J. Chem. Phys*., **6**, 873 (1938)
[46] E. J. W. Verwey, J. T. G. Overbeek and K. van Ness, "Theory of the Stability of Lyophobic Colloids", Elsevier, New York, 1948
[47] J. H. Li, C. Cai, J. R. Li, J. Li, J. Li *et al*., *Molecules*, **23**, 2661 (2018), https://doi.org/10.3390/molecules23102661
[48] M. Rinaudo, *Prog. Polym. Sci*., **31**, 603 (2006), https://doi.org/10.1016/j.progpolymsci.2006.06.001
[49] D. Li, Z. Wei, J. Sun and C. Xue, *Curr. Res. Food Sci*., **5**, 611 (2022), https://doi.org/10.1016/j.crfs.2022.03.008
[50] M. Pascoli, R. de Lima and L. F. Fraceto, *Front. Chem*., **6**, 6 (2018), https://doi.org/10.3389/fchem.2018.00006
[51] J. Jin, C. Liu, H. Tong, Y. Sun, M. Huang *et al*., *Foods*, **11**, 2131 (2022), https://doi.org/10.3390/foods11142131